EVALUATION OF LAND COVER CHANGE IMPACTS ON DISSOLVED IRON FLUX OF THE AMUR RIVER

ONISHI T.[1], SHIBATA H.[2], YOH M.[3], NAGAO S.[4], PARK H.[5] AND SHAMOV V.V.[6]

[1]*River Basin Research Center, Gifu University, Japan*
[2]*Field Science Center for Northern Biosphere, Hokkaido University, Japan*
[3]*Tokyo University of Agriculture and Technology, Japan*
[4]*Low Level Radioactivity Laboratory, Institute of Nature and Environmental Technology,*
Kanazawa University, Japan
[5] *Faculty of Agriculture, Hokkaido University, Japan*
[6]*Institute for Water and Ecological Problem, FEBRAS, Russia*

1. INTRODUCTION

The Amur River is one of the largest trans-boundary rivers that run through the boundary between China and Russia. And origins of the river also come out from Mongolia. The catchment area of the river is 2,050,057km^2 that is the nineth largest river in the world and the total length of the river is 4,350km. Thus, huge amount of fresh water is supplied by the Amur River to the Sea of Okhotsk (Ogi et al., 2001). The Northeast Pacific Ocean including the Sea of Okhotsk is one of the highest primary productive open seas in the world, and it supports high fisheries production of the area. Martin and Fitzwater (1988) found that iron is the limiting nutrient of phytoplankton growth in the Northeast Pacific Ocean. Boyd et al. (2004) showed that, also in the Sea of Okhotsk, dissolved iron plays an important role to maintain the primary production of the area. Though many oceanographers have been thinking that 'Airborne Iron Hypothesis' is a reasonably explanation of main source of this iron, it was unclear since insufficient information on the solubility of aerosol iron and the lack of sequential evidences of aerosol supply and phytoplankton bloom in the open ocean. On the contrary to this, Tovar-Sanchez et al.(2006) suggested that iron inputs from rivers may be substantial in some regions where large rivers discharge to the shelf. Nakatsuka et al. (2007) proposed 'Intermediate – Water Iron Hypothesis' based on observations in the Sea of Okhotsk. Recently, intensive studies to verify this hypothesis finally proved that important part of iron in the Sea of Okhotsk is transported by intermediate water.

In addition to this finding, it is highly probable that important part of this dissolved iron has its origin in the Amur River basin. Iron transported by the Amur River is in the form of dissolved iron, most of which consists of the complex of organic compounds such as fulvic acid and iron. Terrestrial biogeochemical observation verified that wetlands play an important role in producing this dissolved iron. Since wetlands soil is rich in undegraded organic matter and tends to be reductive condition, abundant dissolved iron is produced from wetlands. However, the Amur River basin has been affected by increasing human activity such as conversion of wetland to agricultural land through out the last century. Thus, human activity in the basin might have a great impact on primary productivity of the Sea of Okhotsk by changing dissolved iron productivity of the basin. The aim of this study is to evaluate how human activity will affect dissolved iron productivity of the basin. To achieve this aim, hydrological model that incorporate dissolved iron production mechanism is constructed. And,

by using the constructed model, we evaluate the impact of land cover conversion on dissolved iron productivity of the basin.

2. STUDY SITE

Figure 1 shows the outline of the study site. Main tributaries of the basin are Songhua (Chinese part), Argun, Zeya, Silka, Ussuri. Each basin area is 53,5232km^2, 29,8361km^2, 23,3311km^2, 20,2924km^2, 19,5101km^2. In addition, average river bed slope from the river mouth to Khabarovsk calculated from DEM data which was constructed by SRTM (Shuttle Radar Tomography Mission) is about 1/25,000. Compared to the other large continental river, it is cleared that the Amur river basin is totally very flat. Average precipitation of the Amur river basin is 600 mm. Most of the precipitation is occurred during the period between July to September. The unique characteristics of discharge regime of the Amur river is that two large discharge peaks can be observed in a year (Tachibana et al., 2008). One is formed by snowmelt during the period from April to May, and the other is formed by rainfall during the period from July to September.

Most dominant land cover type is forest that consists of mixed forest, deciduous forest, and coniferous forest. Next, dry land occupies major part of the land cover. Most part of the dryland locates in the Songhua River basin and occupies about 40 percent of the area of Songhua river basin. Main crops are maize, corn and rice (National Bureau of Statistics of China, 1949-2004). Wetland consists about 7 % of the total basin area. And most of the wetland locates along the main course of the Amur river. From on-site investigation and periodical measurements of iron concentration, forest and wetland have a possibility of producing dissolved iron.
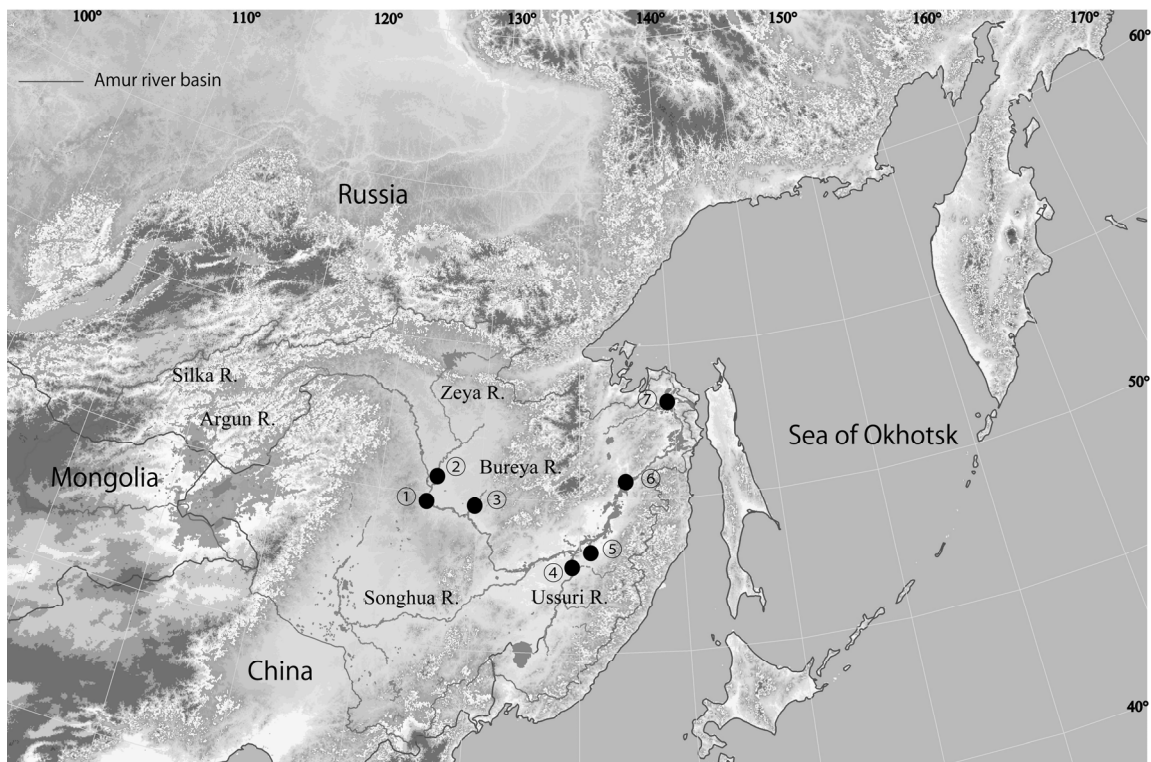
Figure 1 Outline of the study area. Name of main tributaries is shown. Black circles indicate location of observation stations of which data are used in this paper.

As many studies in the Amur-Okhotsk project pointed out, The Amur River experienced drastic land cover change during 20th century. Ermoshin et al. (2007) compiled GIS map of land cover type in two different periods; one is 1930s' and the other is 2000. **Figure 2** shows those two maps. It is clear that wetland decreased and dry land increased. More precisely, wetland and grassland reduced their area approximately 5 point each and the farmland increased approximately 10 point of the whole basin.
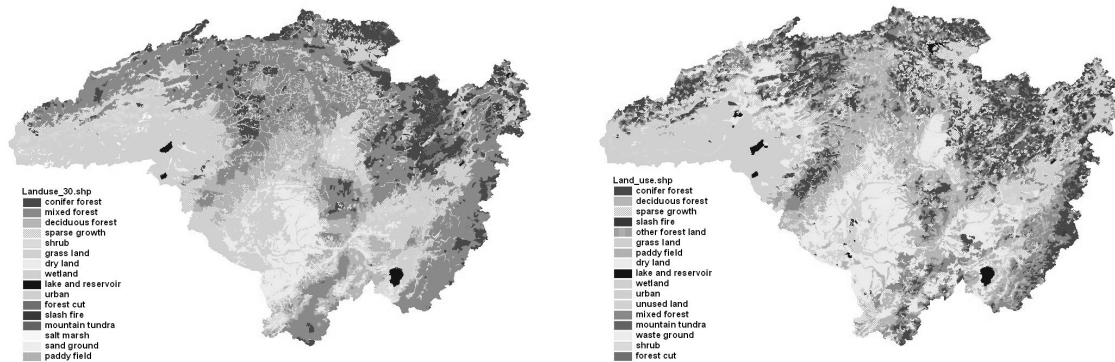

Figure 2 Land cover type in 1930's (left) and 2000 (right)

3. OBSERVATION DATA

Observation data consists of discharge and dissolved iron data. We obtained discharge data at main course and several main tributaries of the Amur River basin from Federal Service for Hydrometeorology and Environmental Monitoring (ROSHYDROMET) and Global Runoff Data Center (GRDC) in Koblenz, Germany (http://grdc.bafg.de) .

We obtained two kinds of dissolved iron concentration data. One is long term dissolved iron concentration data obtained from the Federal Service for Hydrometeorology and Environmental Monitoring (ROSHYDROMET) in Russia (HYDROMET-FE). The other is relatively short-term data measured by our research group mainly in the Sanjiang plain in China (SANJIANG-FE). All observation points used for analysis are also shown in Figure 1. River discharge was also estimated based on the measurements of river flow velocity at several points in each river in ROSHYDROMET data. Land cover types of each watershed include forest, grassland, scrub, wetland, and agricultural land. Analysis method of dissolved iron concentration by ROSHYDROMET and us is different. Collected water was filtered using 0.45mm filter and filtered water was analyzed by using photometry with ROSHYDROMET data. On the other hand, our data was filtered also using 0.45mm filter but filtered water was analyzed by using ICP-MS spechtrometer.

For the calculation of hydrological model, both precipitation rate and evapotranspiration rate are needed as forcing data. Thus APHRODETE data set (Takashima et al., 2009) was used for calculation of precipitation amount. Spatial and temporal resolution of data set are 0.5°×0.5°, and 1 day respectively. The data set covers the period of 1980 to 2002. On the other hand, NCEP - DOE reanalysis-2 data were used for estimation of evapotransipiration rate. The spatial resolution of NCEP – DOE reanalysis data is 2.5°×2.5°.

4.1 Model Structure

The constructed model is based on the TOPMODEL concept (Beven and Kirkby, 1979). While TOPMODEL was originally developed to simulate runoff from a small scale catchment, its concept is also used in global scale Land Surface Models such as MATSIRO (Takata et al., 2003). The model consists of two modules; one for dealing with the physical process that calculates runoff (TOP-RUNOFF), and the other for dissolved iron production processes (TOP-FE). Schematic diagram of the model is shown in **Figure 3**.

S_{rz} [m]: root zone storage, S_{uz} [m]: storage in the unsaturated zone,
q_v [m s^{-1}]: drainage flux from unsaturated zone to saturated zone.
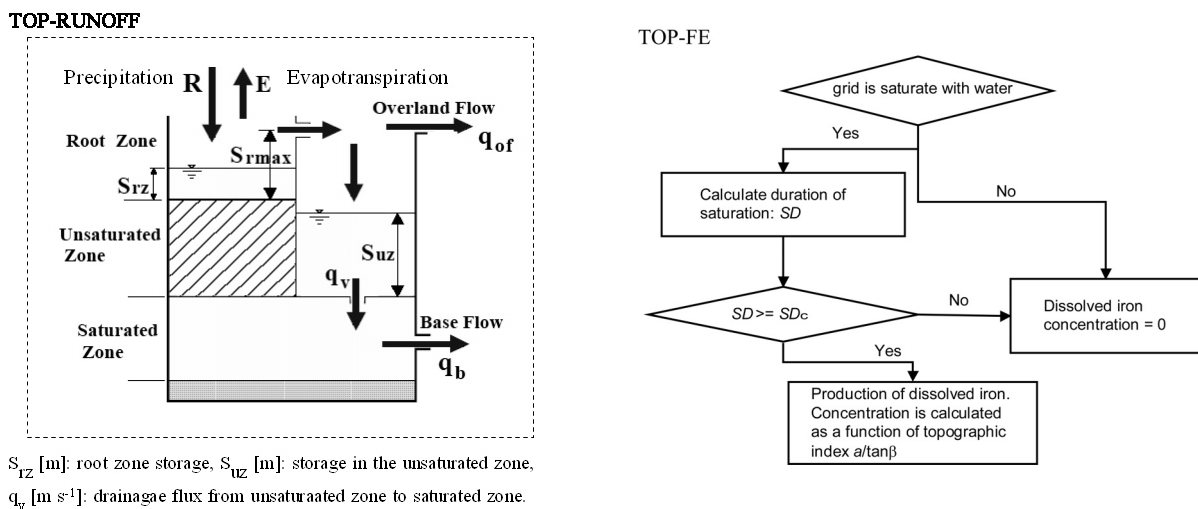
Figure 3 Schematic diagram of the model. Runoff calculation module TOP-RUNOFF is shown in the left figure, and dissolved iron concentration calculation module TOP-FE is shown in the right figure.

In the TOP-RUNOFF module, as well as the basic structure that is the same as the original TOPMODEL structure, two processes were taken into account. One is the inflow of surface water runoff from surrounding lands into the wetlands. This process was simply formulated as the equal addition to the wetlands of the amount of surface runoff from grids except for paddy fields. The second process involved water management practices for paddy fields. This management was taken into account as the overflows from paddies when the ponding depth exceeded the prescribed threshold value PDc [m] that is equal to the depth of paddy field levee. Thus, the modeling algorithm

Figure 4 Water management practice for paddy fields.

assumed that artificial drainage such as mid-summer drainage was not practiced in the basin. Though some exceptions might exist in actual water management, the above mentioned formulation can be justified by information obtained from field observations and inquiries of farmers. Finally, total runoff from each grid is routed using TRIP (Oki and Sud, 1998). River
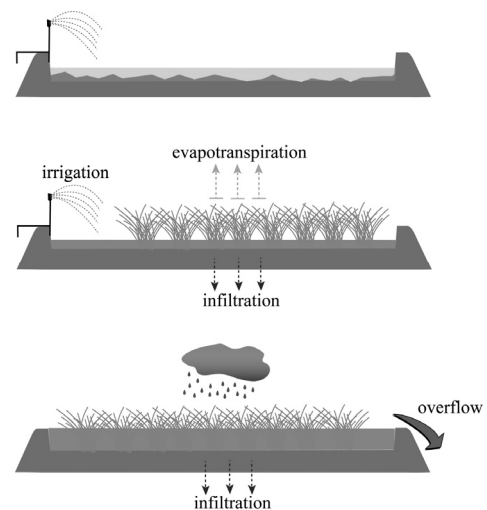
network used for runoff routing is shown in **Figure 4**.

In the TOP-FE module, the degree to which dissolved iron is produced is formulated as the function of the duration time for saturation; defined as the length of continuously saturated days. In the model, when both root zone deficit and saturation deficit of each grid reached zero, the grid was considered as saturated. If the saturation duration time of a grid became larger than the threshold value SDc, then dissolved iron is considered to be produced at a prescribed constant rate. The concentration of the dissolved iron produced is formulated as a function of the topographic index $a/\tan\beta$ (Andereson and Nyberg, 2008, Dillon and Molot, 1997). Here, a is defined as drainage area of each calculation grid and β is defined as slope angle of each grid. The function was formulated as an exponential curve with different parameters according to land cover type (Onishi et al., 2009) that is shown in **Figure 6**.
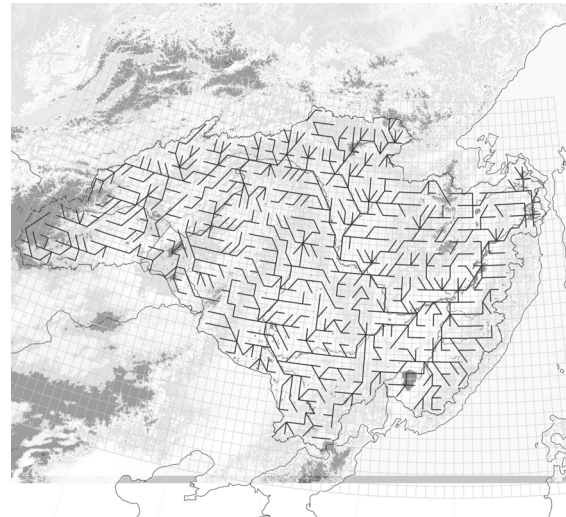

Figure 5 River network used for runoff routing of calculated discharge from each grid
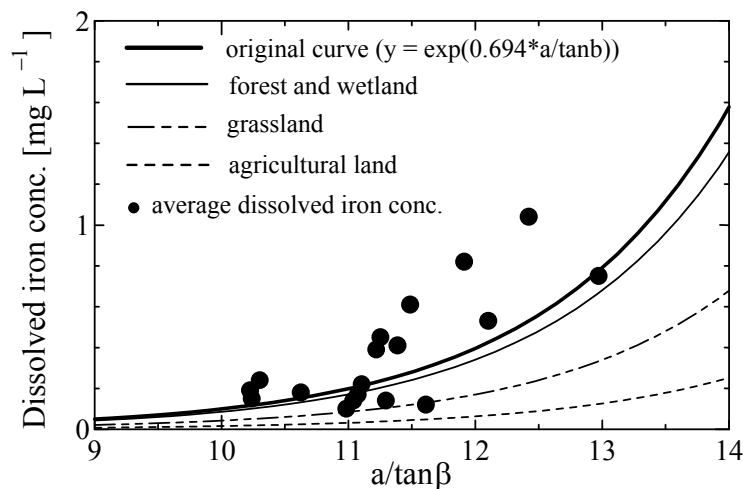

Figure 6 Dissolved iron concentration curve with regards to topographic index a/tanβ.

4.2 Experimental design of land cover change

Two typical land cover conversion scenarios were set. One is conversion from wetland to agricultural land. The other is wild fire excluding peat fire. In addition, dissolved iron concentration under the 1930s' land cover condition was also simulated. Conversion ratio of each scenario is 50%, 100% for wetland conversion, and 10% and 30% for forest fire. In all scenarios, grids that correspond to the conversion ratio in each scenario were selected randomly and converted to agricultural lands or wild fire. Effect of wild fire on productivity of dissolved iron is assumed as negative. Based on the comparative studies of dissolved iron productivity of natural forests and burnt forest, it was assumed that dissolved iron

productivity would decrease as half as that of original natural forest (personal communication with Dr. H. Shibata). The time length of all experiments was 10 years using the climate data during the period from 1981 to 1990. Average annual dissolved iron flux under the different land cover conversion scenarios was compared.

4.3 Input parameters

Input parameters are listed in **Table 1**. Spatial resolution of parameters is different. The most coarse data is NCEP - DOE reanalysis-2 data that is used as climate forcing data except for precipitation.

Table1 List of input parameters

Symbol	Description	Unit	Resolution	Value	Source
Prescribed with horizontal distribution					
	land cover type	-	1000m		AO[a]
	soil type	-	1°		ISLSCP2
	elevation	m	1000m		SRTM
$a/\tan\beta$	topographic index	m	1000m		SRTM
prescribed with land cover type					
LAI	leaf area index	m^2/m^2	1000m		ORNL DAAC
	height of canopy top and bottom	m	1000m		ORNL DAAC
	surface conductance	m/s	1000m		Kondo(1994)
	aerodynamic conductance	m/s	1000m		Kondo(1994)
prescirbed with soil type					
T_0	saturated hydraulic conductivity	m/s	1°		ISLSCP2
prescribed as constant					
szm	scaling parameter for runoff	m	-	0.001	-
SR_{max}	maximum root zone deficit	m	-	0.01	-
t_d	time constant for recharge to the saturated zone	m/h	-	0.1	-
chv	channel routing velocity	m/s	-	0.5	-
rv	river routing velocity	m/s	-	0.5	-
Cw	snow water retention capacity	-	-	0.1	-
T_s	threshold temperature for 100%snow	K	-	2.0	Beven (2000)
T_r	threshold temperature for 100%rain	K	-	4.5	Beven (2000)
T_m	threshold temperature for snow melt	K	-	0.0	Beven (2000)
PD_c	upper limit of ponding depth of paddy fields	m	-	0.1	-
SD_c	threshold for starting of dissolved iron production	day	-	1	-

a: Product of Amur-Okhotsk project

Symbol	Description	Unit	Resolution	Array	Source
U_a	zonal wind velocity	m/s	2.0°	-	NCEP2
V_a	meridional wind veolocity	m/s	2.0°	-	NCEP2
T_a	atmospheric temperature	K	2.0°	-	NCEP2
q_a	atmospheric humidity	kg/kg	2.0°	-	NCEP2
R_d	downward radiation	W/m^2	2.0°	S/L[a]	NCEP2
R_u	upward radiation	W/m^2	2.0°	S/L	NCEP2
P	precipitation	mm/day	0.5°	-	Aphrodite

[a] S:shortwave radiation, L:longwave radiation

5. RESULTS

5.1 Model calibration and validation

Figure 7 shows comparison between observed and calculated discharge in monthly at three different observation stations along the main course of the Amur river. The result shows fairly good agreement of calculating discharge with observed value, though any calibration process was not applied. **Figure 8** is the comparison of observed and calculated dissolved iron flux in annual at the Khabarovsk station during the period between 1980 and 1990.
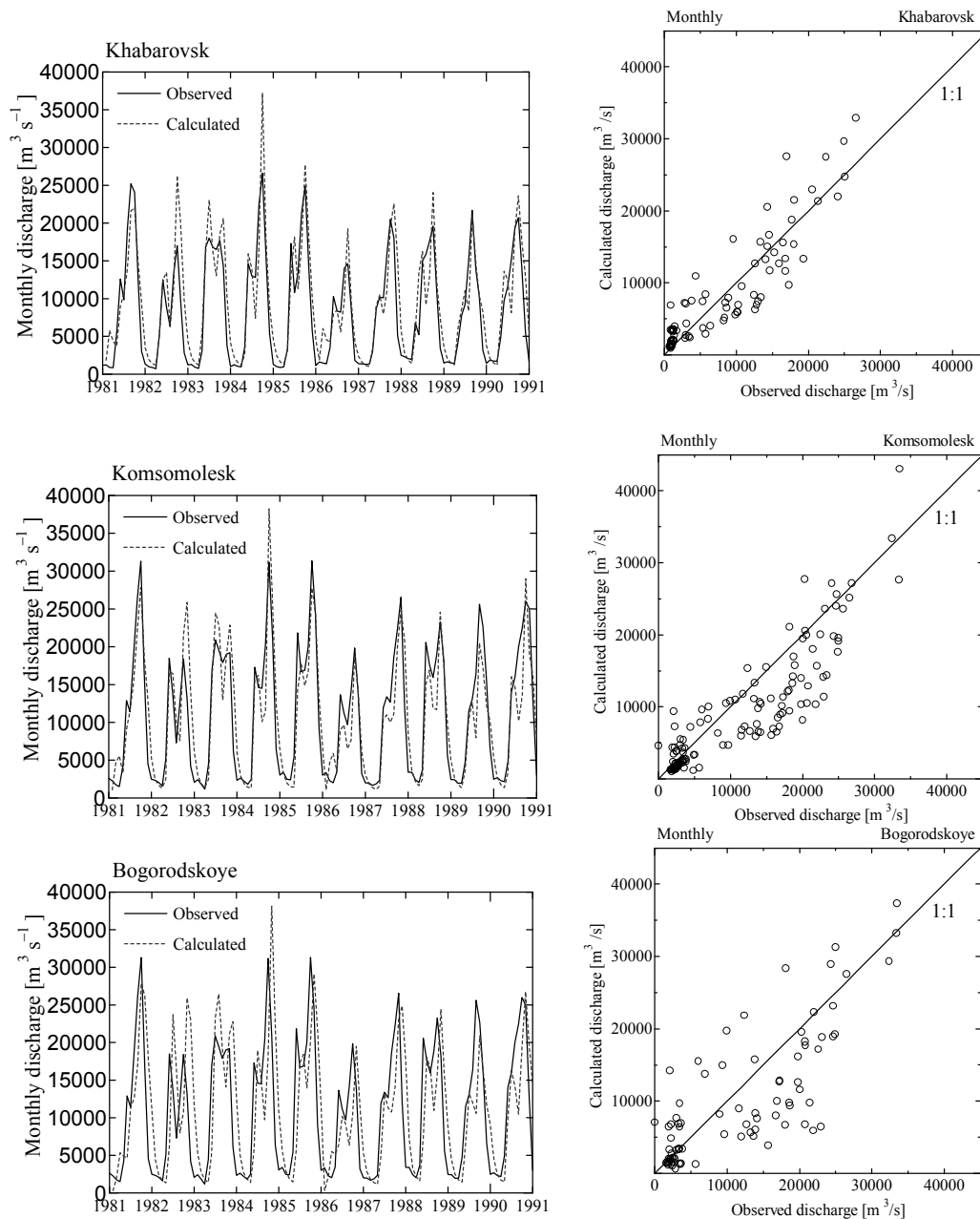

Figure 7 Observed and calculated monthly discharge along the main course of the Amur River Location of Khabarovsk, Komsomolesk, and Bogorodoskoye is corresponding to ⑤, ⑥, ⑦ in the Figure 1. Figures in left column are time series and figures in right column are plotting of the same data.
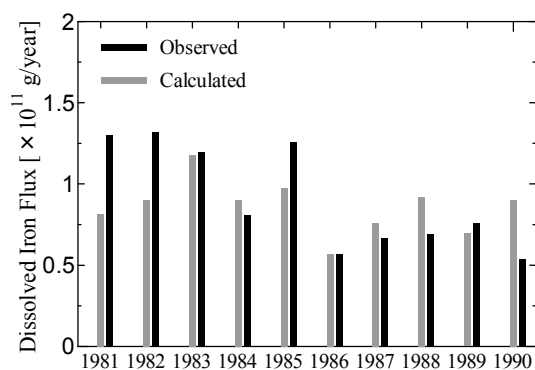
Figure 8 Comparison of calculated and observed dissolved iron flux at Khabarovsk. Location of Khabarovsk is ⑤ in the Figure1.

Validation period and the time when the land cover condition was compiled are not same. However, statistical data of the Heilongjiang province (National Bureau of Statistics of China, 1949-2004) suggested that expansion of agricultural land area reached stable after 1980. Thus, it is assumed that land cover condition of 1980s' and 2000 can be considered as being similar. Though the result shows non-negligible difference in some years, calculated dissolved iron flux shows good agreement with observed values in general.

6. LAND COVER CONVERSION EFFECT ON DISSOLVED IRON FLUX

Figure 9 shows the dissolved iron flux as determined by numerical simulation near the mouth of the Amur River and several main tributaries (Zeya, Bureya, Songhua, and Ussuri). The results suggest that the impact of agricultural development on dissolved iron flux is much greater than that of forest fires. This supports the idea that wetland conversion plays an important role in dissolved iron productivity, even though the areal extent of wetlands is not so large. Complete conversion of wetlands in the basin might result in a decrease in dissolved iron flux of approximately 20% compared with present conditions. Our experiments also indicate that dissolved iron flux under the land-cover conditions of the 1930s was more than 20% higher than under present land-cover conditions.

Examining the extent to which each of the tributaries contribute to the change in total dissolved iron flux shows that the decrease of wetlands within the Chinese part of the catchment has had a great impact on the dissolved iron productivity of the basin. In contrast, our experiments show that the influence of wild fire has not had much impact, because of the low dissolved iron productivity characteristics of forested regions. However, in addition to forest fires, there is some evidence that the scale of fires in peat land is also extensive in the basin. Whether such peat fires results in a distinguishable change in dissolved iron production is not clear. If we assume that peat fire also has a negative effect on dissolved iron productivity, it may significantly decrease the total dissolved iron flux.
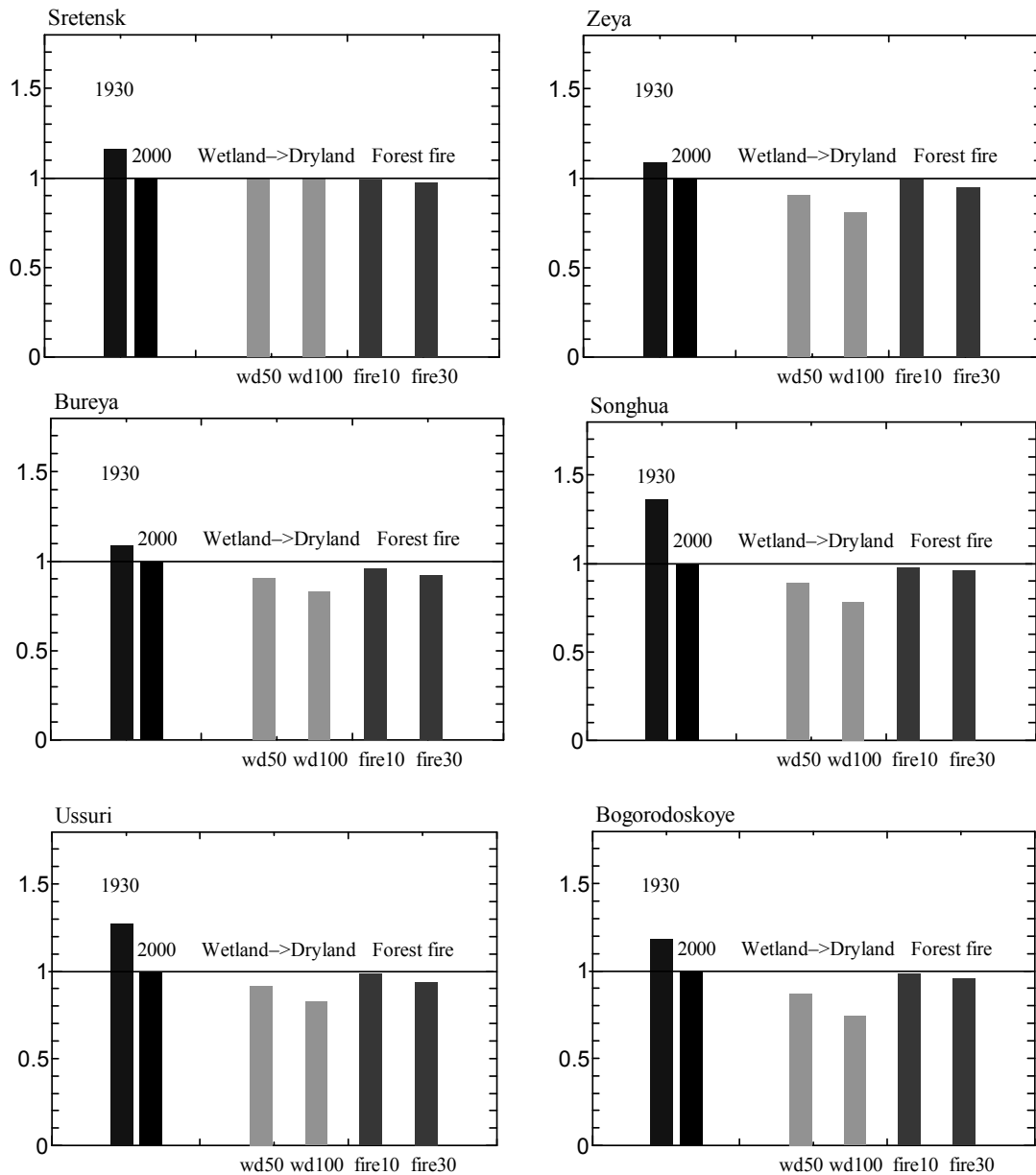
Figure 9 Simulated results of the effect of land cover conversion on dissolved iron productivity in the basin (wd50: 50% converted, wd100: 100% converted, fire10: forest fire area is 10%, fire20: forest fire area is 20%). The vertical axis corresponds to relative increase/decrease compared with dissolved iron flux under the present land cover conditions.

Until now, the constructed model has not included the effect of slow changes in soil chemical characteristics that may result from the conversion of wetlands to agricultural lands. This effect might occur over a discrete time period due to gradual changes in soil chemical properties that occur after the conversion. However, our model formulates such an effect as being abrupt. Therefore, in observational data, we might expect some delay in the timing of chemical or physical responses to land-cover conversion.

Dissolved iron from the Amur River basin supplies a huge amount of iron to the Sea of Okhotsk. This iron is one of the most important factors supporting primary production in the sea. However, the effect of land-cover conversion on the primary production of the sea has not yet been resolved. This effect can be projected by coupling hydrological and ocean circulation

model. Coupling these two models beyond the boundary of land and ocean to simulate water movement seamlessly is the next challenging subject.

ACKNOWLEDGEMENT

REFERENCE

Anderson J.-O. L. Nyberg (2008): Spatial variation of wetlands and flux of dissolved organic carbon in boreal headwater streams, Hydrological Process, 22, pp.1965-1975

Beven K.J., and Kirkby (1979): A physically based, variable contributing area model of basin hydrology, Hydrol. Sci. Bull., 24, pp.43-69

Boyd P.W., Law C.S., Wong C.S., Nojiri Y., et al. (2004): The decline and fate of an iron-induced subarctic plankton bloom, Nature, 428, pp.549-553

Dillon P.J. and L.A. Molot (1997): Effect of landscape form on export of dissolved organic carbon, iron, and phosphorous from forested stream catchment, Water Resour. Res. Vol.33, pp.2591 - 2600

Ermoshin V.V. and S.S. Ganzey, A.V. Murzin, N.V. Mishina and E.P. Kudryavtzeva (2007): Creation of GIS for Amur River basin: the basic geographical information, Annual Report on Amur-Okhotsk Project, No.4, pp.151-159.

GRDC (2006): The global runoff data centre, D-56068 Koblenz, Germany

Martin J.H., S.E. Fitzwater (1988): Iron deficiency limits phytoplankton in the northeast Pacific subarctic, Nature, 311, pp.341-343

Migration behavior of Fe in the Amur river basin, Report on Amur-Okhotsk Project, No.4, pp. 37-48 (http://www.chikyu.ac.jp/AMORE/)

Nakatsuka T., and all members of research group 1 and 2 (2007): How can the iron from amur river support the primary productivity in North Pacific Ocean?, Report on Amur-Okhotsk Project, No.4, pp.25-36 (http://www.chikyu.ac.jp/AMORE/)

National Bureau of Statistics of China (1949-2004) : Statistical year book of Heilongjiang Province

Ogi M., Y. Tachibana, F. Nishio, and M.A. Danchenkov (2001): Does the fresh water supply from the Amur River flowing into the Sea of Okhotsk affect sea ice formation?, J.

Meteorol. Soc, Jpn., 79, pp.123-129

Onishi T., Y. Muneoki, H. Shibata, S. Nagao, M. Kawahigashi, V. V. Shamov (2009): Identification of macroscopic index of dissolved iron productivity and its flux from different land cover type in the Amur River basin (submitted)

Oki T., and Y.C. Sud (1998): Design of Total Runoff Integrating Pathways (TRIP)—A Global River Channel Network, Earth Interactions, 1(2), pp.1-37

Tachibana, Y., K. Oshima, and M. Ogi (2008): Seasonal and interannual variations of Amur River discharge and their relationships to large-scale atmospheric patterns and moisture fluxes, Journal of Geophysical Research, 113, D16102.

Takashima, H., A. Yatagai, H. Kawamoto, O. Arakawa, and K. Kamiguchi (2009): Hydrological balance over northern Eurasia from gauge-based high-resolution daily precipitation data, M. Taniguchi (eds.), From Headwaters to the Ocean: Hydrological Change and Watershed Management, Taylor & Francis, pp.35-41

Takata K., S. Emori and T. Watanabe (2003): Development of the minimal advanced treatments of surface interaction and runoff, Global and Planetary Change, pp.209-222

Tovar-Sanchez, A., Sãnudo-Wilhelmy, S. A., Kustka, A. B., Agusti, S., Dachs, J., Hutchins, D. A., Capone, D. G., Duarte, C. M.(2006): Effects of dust deposition and river discharges on trace metal composition of Trichodesmium spp. in the tropical and subtropical North Atlantic Ocean, Limnol. Oceanogr., 51(4), 1755–1761